Analysis of Coordinated HVDC Control for Power Oscillation Damping

Joakim Björk
KTH Royal Institute of Technology
Stockholm, Sweden
joakbj@kth.se

Karl Henrik Johansson
KTH Royal Institute of Technology
Stockholm, Sweden
kallej@kth.se

Lennart Harnefors
Corporate Research, ABB
Västerås, Sweden
lennart.harnefors@se.abb.com

Robert Eriksson
R&D, Svenska kraftnät
Sundbyberg, Sweden
robert.eriksson@svk.se

***Abstract*—Controlling the active power of high-voltage dc (HVDC) transmission that interconnects two asynchronous ac grids can be used to improve the power oscillation damping in both of the interconnected ac systems. Using one HVDC link, achievable performance are limited since control actions may excite modes of similar frequencies in the assisting network. However, with coordinated control of two or more HVDC links, the limitations can be circumvented. With decoupling control the system interactions can be avoided all together. This paper investigates the conditions suitable for decoupling control. It is also shown that decoupling between system modes can be achieved using a proportional controller. The control method is compared to decentralized and $\mathcal{H}_2$ optimal control. The best control method for different system topologies is investigated by looking on input usage and stability following dc link failure.**

***Index Terms*—Decoupling control, HVDC transmission control, interarea oscillations, mimo control, multivariable interaction, power oscillation damping.**

I. Introduction

Poor damping of interarea or power oscillation modes often occur when transmitting large amounts of power over long distances. This may limit the net transfer capacity (NTC) of traditional ac systems. High-voltage dc (HVDC) is an attractive alternative to traditional ac transmission over long distances. In addition to lower transmission losses, the high controllability of active power (and reactive power if voltage source converter (VSC) technology is used), allows the utility to actively improve power system stability, thereby increasing the NTC of existing ac lines [1]–[7]. Further, HVDC transmission allows for the connection of asynchronous grids. An interconnected energy market is crucial in the transition towards a renewable and sustainable power sector. Since this expansion may lead to even higher demands of transmission capacity, it is important that power oscillation damping (POD) is addressed.

Point-to-point HVDC lines parallel to ac lines that interconnect two oscillating areas are efficient in improving the POD. This has been shown both in theory and practice [6]–[9]. In [6] active power modulation of the Pacific HVDC Intertie (PDCI) is successfully implemented to improve POD in the western North American power system, thereby increasing the NTC of the parallel Pacific AC Intertie. Wide-area measurement systems can be used to improve POD performance. In [7] it was shown that the relative feedback between the two dc terminals of the PDCI gives better robustness properties than local frequency or ac power flow measurements. In [8] the robustness and performance of wide are measurement system (WAMS) based POD controllers are evaluated using a probabilistic methodology. A modal linear quadratic Gaussian controller is implemented to target weakly damped modes in the system, controlling two VSC-HVDC links. In [9] a linear matrix inequality based method for optimal placement of multiple HVDC lines within a meshed ac network is presented.

Coordinated control of multi-terminal HVDC (MTDC) offers potentially more controllability and flexibility than point-to-point HVDC. With few active systems in operation today, MTDC is receiving a lot of research focus [2], [10]–[12]. In [10] a decentralized control method is developed to improve POD through a MTDC system connected to an ac grid. Active power is controlled at the dc terminal with strongest controllability of the oscillatory mode. Voltage droop controllers, at the remaining dc terminals, are then tuned to maximize POD without the need of communication between the terminals. In [11] a cascaded control strategy is developed to provide virtual inertia to an ac network by utilizing energy stored in dc capacitors and the inertia of the wind turbines. It was shown that utilizing dc capacitors in first hand could help increase wind power production by allowing for a better power point tracking. However, it was shown that HVDC capacitor value had little effect on overall inertia support compared to the kinetic energy stored in the wind turbines. In [12] the interaction between an ac network and an MTDC system integrated with wind power is analyzed. Normally, electromechanical dynamics are much slower than the converter control of the MTDC. However, it was shown that the dc voltage control, under certain conditions, may cause strong dynamical interactions between the MTDC and AC systems, degrading POD performance. Most of the literature focus on the dc and inverter dynamics, or HVDC transmission embedded in single ac grid. To complement existing research, this work instead focuses on the electromechanical interactions that may occur due to HVDC active power control between

This work was done under the PhD program in the digitalization of electric power engineering, School of Electrical Engineering and Computer Science, KTH Royal Institute of Technology, Sweden.

The work was supported in part by the Knut and Alice Wallenberg Foundation, the Swedish Research Council, and the Swedish Foundation for Strategic Research.

978-1-5386-6705-7/18/$31.00 ©2018 IEEE

asynchronous ac grids.

One concern that arises when utilizing HVDC active power control for POD is that the interarea mode of the assisting network may be excited [13]. Since poorly damped interarea modes usually fall in the same frequency ranges [1], control methods should avoid unnecessary excitation of weekly damped modes. Interactions can be mitigated by incorporating energy storage from integrated wind power or large capacitor banks in the dc system [11], [12]. In this work, a solution that does not require dc energy storage is proposed. In [13] it was shown that, although propagating the disturbance to the assisting network, the overall POD can be improved in both ac networks. In earlier work by the authors [14] it has been shown that the limiting performance factor for such a control strategy is the proximity of interarea modal frequencies between the two ac networks. A higher feedback gain improves POD of both ac networks, but also moves the frequency of the interarea modes, and their eigenvalues, closer to each other thereby reducing controllability through modal interaction. With a higher system inertia, stronger control action is needed to improve POD, making this effect independent of system inertia.

With additional HVDC lines, the limitations imposed by modal interactions can be circumvented. Since multiple HVDC connection between asynchronous ac networks are common today, improvement of system dynamical performance using coordinated control can be achieved without the need for any additional hardware installations. The main contribution of this paper is to show how the system topology affects multivariable interactions in the HVDC-interconnected system. It is shown that decoupling control, avoiding the interaction between selected interarea modes all-together, can be achieved using a proportional controller. The decoupled controller is compared to a decentralized, single line equivalent, as well as a $\mathcal{H}_2$ optimal controller. Suitability of the different control methods is analyzed with respect network topology and sensitivity to dc link failures.

The remainder of the paper is organized as follows. In Section II a model of two simple ac networks interconnected with two HVDC-lines are defined. In Section III single-line, decentralized, decoupling, and $\mathcal{H}_2$ control methods are compared. The robustness of the control methods are investigated with respect to dc link failure. In Section IV the decoupled control is implemented on the Nordic-32 model. Section V concludes the paper with some discussion of future work.

II. Model

Consider the system shown in Fig. 1. The dominant interarea mode of each ac network is represented using the simplified two-machine model presented in [13] where each machine represents an aggregation of synchronous machines. Electromechanical dynamics of ac network $i \in \{1,2\}$ is given by the swing equation of each machine $j \in \{1,2\}$

$$\dot{\delta}_{ij} = \omega_{ij},\ M_{ij}\dot{\omega}_{ij} = \Delta P_{ij} - \frac{V^2}{X_{ij}}\sin(\delta_{ij} - \theta_{ij})$$

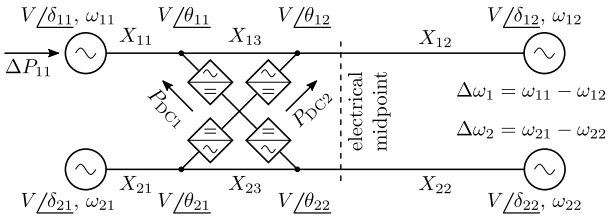

Fig. 1. Two asynchronous two-machine networks interconnected with point-to-point HVDC lines in a one-sided configuration where both HVDC terminals are on the same side of the electrical midpoint in each ac network.

where state-variables δ_{ij} and ω_{ij} represents machine voltage phase angle and frequency respectively, M_{ij} machine inertia, X_{ij} line reactance, and ΔP_{ij} the difference between injected power and load at machine bus ij. All buses are assumed to have a constant voltage amplitude V for the time frame of interest. For the analysis, higher order dynamics such as voltage regulators, governors, and machine damper windings are ignored. Since load dynamics ΔP_{ij} are not of interest in the analysis, loads are assumed to act directly on generator states. However, the ac voltage phase angle θ_{ij} at the HVDC terminals, affected by HVDC active power injections $\Delta P_{\mathrm{DC}h},\ h \in \{1,2\}$, are given by Kirchoff's current law

$$P_{\mathrm{DC}h} + \frac{V^2}{X_{ij}}\sin(\delta_{ij} - \theta_{ij}) - \frac{V^2}{X_{i3}}\sin(\theta_{ij} - \theta_{il}) = 0$$

where $l \in \{1,2\},\ l \neq j$. Representing the swing mode using the relative phase and machine speeds $\Delta\delta_i = \delta_{i1} - \delta_{i2}$ and $\Delta\omega_i = \omega_{i1} - \omega_{i2}$ the following lti representation is obtained

$$\begin{bmatrix}\Delta\dot{\delta}_i \\ \Delta\dot{\omega}_i\end{bmatrix} = \underbrace{\begin{bmatrix}0 & 1 \\ \frac{-V^2(M_{i1}+M_{i2})}{M_{i1}M_{i2}X_{i\Sigma}} & 0\end{bmatrix}}_{A_i}\begin{bmatrix}\Delta\delta_i \\ \Delta\omega_i\end{bmatrix} + \underbrace{\begin{bmatrix}0 & 0 \\ b_{i1} & b_{i2}\end{bmatrix}}_{B_i}\underbrace{\begin{bmatrix}P_{\mathrm{DC1}} \\ P_{\mathrm{DC2}}\end{bmatrix}}_{u}$$

where $X_{i\Sigma}$ is the series reactance between the machine buses in network i, A_i, and B_i is the system state and input matrix respectively. The input u are the controlled active power injections of the two dc links. As an example, the input matrix

$$B_1 = \begin{bmatrix}0 & 0 \\ \frac{M_{12}(X_{12}+X_{13})-M_{11}X_{11}}{M_{11}M_{12}X_{1\Sigma}} & \frac{M_{12}X_{12}-M_{11}(X_{11}+X_{13})}{M_{11}M_{12}X_{1\Sigma}}\end{bmatrix} \quad (1)$$

is obtained for network 1 in Fig. 1.

Let $y_i = \Delta\omega_i$ be the measured output signal. The transfer function G_i from u to y_i then becomes

$$G_i = \begin{bmatrix}0 & 1\end{bmatrix}(sI - A_i)^{-1}B_i = \frac{s}{s^2 + \Omega_i^2}\begin{bmatrix}b_{i1} & b_{i2}\end{bmatrix}$$

where

$$\Omega_i = \sqrt{\frac{X^2(M_{i1} + M_{i2})}{M_{i1}M_{i2}X_{i\Sigma}}}$$

is the undamped frequency of network i.

The HVDC-interconnected system to be controlled, is represented by the transfer function

$$G = \begin{bmatrix}G_1 \\ -G_2\end{bmatrix} = \begin{bmatrix}\frac{s}{s^2+\Omega_1^2} & 0 \\ 0 & \frac{s}{s^2+\Omega_2^2}\end{bmatrix}\begin{bmatrix}b_{11} & b_{12} \\ -b_{21} & -b_{22}\end{bmatrix}. \quad (2)$$

A. Electrical Midpoint

The electrical midpoint is the mass-weighted electrical center between the two areas. This is the point where the elements b_{ih} in the input matrix (1) changes sign. Close to the electrical midpoint, where $\text{sgn}(b_{ih})$ might be uncertain, e.g., due to changing ac power flows, high feedback gains should be avoided to not risk destabilizing the system (2).

B. Model Parameters for the One-Sided HVDC-Configuration

Consider two identical HVDC-interconnected ac networks in a *one-sided configuration* as seen in Fig. 1, where

- undamped modal frequencies $\Omega_1 = \Omega_2 = 0.5\,\text{Hz}$,
- $a_{ih} \in [0, 1]$ represent the relative electrical position of HVDC terminal ih s.t. $a_{11} = X_{11}/X_{1\Sigma}$ and $a_{22} = (X_{21} + X_{23})/X_{2\Sigma}$. The HVDC terminal positions in Fig. 1 are given $a_{11} = a_{22} = 0.2$, and $a_{12} = a_{21} = 0.3$,
- constant voltage $V = 1\,\text{p.u.}$ is assumed at all buses,
- machines are identical with inertia constants $M_{ij} = 2HS_r/\omega_n$ where, for each machine, rated power $S_r = 4\,\text{p.u.}$, inertia time constant $H = 6\,\text{s}$, and $\omega_n = 2\pi f_n$ where $f_n = 50\,\text{Hz}$ is the nominal system frequency.

III. Control Design

It is clear that control of u_1 will have most effect on y_1 while u_2 have most effect on y_2. The performance of the controllers is tested by simulating a load step at machine bus 11. Results are compared in Fig. 2 where all controllers have a constant gain of $k = 1\,\text{Hz}^{-1}$.

A. Single-Line Control

To counteract ac power flows and improve POD, the dc active power is controlled uniformly for the two HVDC links

$$u_1 = u_2 = \begin{bmatrix} -k & k \end{bmatrix} y.$$

As shown in [14], the achievable POD performance will be limited by modal interactions. Increasing the gain will cause system eigenvalues corresponding to the two interarea modes to approach each other. The controllability of the interarea modes are thereby lost. In this case, since $\Omega_1 = \Omega_2$ the interarea modes are uncontrollable no matter the feedback gain. The only achievable benefit is sharing of the disturbance between the two networks as can be seen in Fig. 2a.

B. Decentralized Control

Decentralized control works well if the condition number of G is small and the system is close to diagonal i.e., the controllability from the chosen input-output pairings are high relative to the other input-output combinations [15]. For the considered one-sided system configuration, satisfactory decentralized control is realized with the diagonal controller

$$u = \begin{bmatrix} -k & 0 \\ 0 & \text{sgn}(b_{22})k \end{bmatrix} y, \ \text{sgn}(b_{11}) \triangleq 1. \tag{4}$$

In Fig. 2b it is seen that the decentralized control method manages to circumvent the limitations of the single-line control. Since a decentralized control method makes no attempt to cancel interactions in G, resulting performance may be poor if these are considerable.

C. Decoupling Control

By shaping $\tilde{G} = GW$ to be a diagonal system, independent control of each input-output combination can be realized using a diagonal controller. Each control-loop can be tuned independently using siso methods for the corresponding input-output path [15]. The pre-compensator W can be chosen in many ways[1]. Here we choose

$$W = \begin{bmatrix} 1 & \frac{-b_{12}}{b_{11}} \\ \frac{-b_{21}}{b_{22}} & 1 \end{bmatrix} \tag{5}$$

and thus

$$\tilde{G} = \begin{bmatrix} \frac{s}{s^2+\Omega_1^2} & 0 \\ 0 & \frac{s}{s^2+\Omega_2^2} \end{bmatrix} \begin{bmatrix} b_{11} - \frac{b_{12}b_{21}}{b_{22}} & 0 \\ 0 & -\left(b_{22} - \frac{b_{12}b_{21}}{b_{11}}\right) \end{bmatrix}.$$

Disturbance rejection, comparable to the decentralized controller (4), is achieved using

$$u = W \begin{bmatrix} -k & 0 \\ 0 & \text{sgn}(b_{22})k \end{bmatrix} y = Ky, \ \text{sgn}(b_{11}) \triangleq 1. \tag{6}$$

With a decoupling controller, the excitation of the interarea mode in the assisting system is avoided as seen in Fig. 2c. The downside of the decoupling control method may be an increased input usage since one link is controlled to counteract the effect on the assisting network. If G is ill-conditioned (large condition number), then off-diagonal elements in G are large. Thus, no obvious input-output combination exist to control the multivariable system. This makes it unsuitable for both decoupling and decentralized control.

Remark 1: Changing ac power flows, system inertia or the connection/disconnection of ac transmission lines may affect the decoupling performance of the controller since the electrical midpoint or the HVDC terminals position relative to each other may change. However, such uncertainties are unlikely to be severe enough to cause instability if the system is eligible for decoupling control in the first place.

Remark 2: Decoupling using a constant matrix is possible since we represent the interarea mode using individual state variables and assume that these are available from measurement. Basically, we are decoupling the system at the frequency of the interarea mode. The proposed decoupling controller can be generalized to higher order systems (this is done for the implementation in Section IV) but this falls outside the scope of this paper.

D. $\mathcal{H}_2$ Optimal Control

The $\mathcal{H}_2$ controller (essentially an lqg controller [15]) is obtained as the controller K that minimizes the $\mathcal{H}_2$ norm of the closed-loop system shown in Fig. 3, from input variables ΔP and d_y to performance variables z_y and z_u. For a dynamical response similar to that of the decentralized and decoupled controller, the controller is tuned with

- external inputs $|\Delta P_{ij}| \leq 0.4\,\text{p.u.}$ and $|d_{yi}| \leq 5\%, \ i, j \in \{1, 2\}$ over all frequencies,
- performance weights $W_z = 1$ and $W_u = 5$.

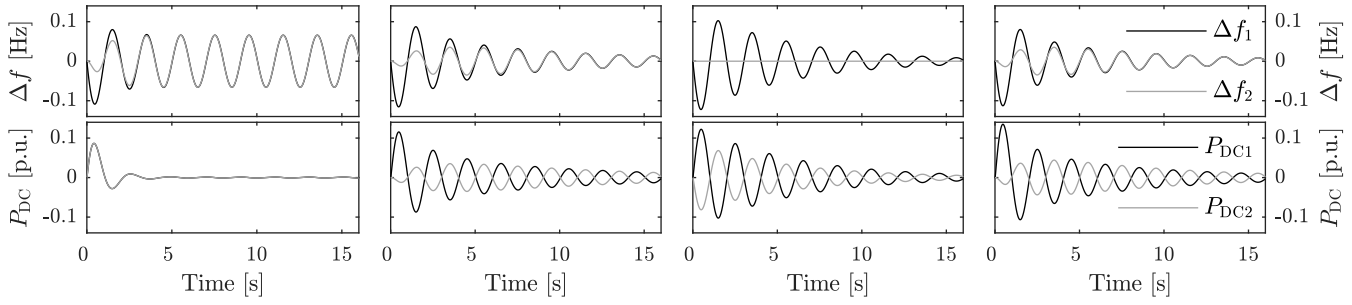

(a) Single-Line Control (b) Decentralized Control (c) Decoupling Control (d) $\mathcal{H}_2$ Optimal Control

Fig. 2. Comparison between different control strategies on the HVDC-interconnected system seen in Fig. 1. Relative machine speeds $\Delta f_i = f_{i1} - f_{i2}$ and resulting dc active power injections following a 0.4 p.u. load step at machine bus 11.

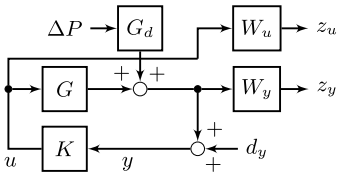

Fig. 3. The closed-loop feedback system used for $\mathcal{H}_2$ synthesis. Block G_d represent the transfer function from machine bus disturbances to relative machine speeds.

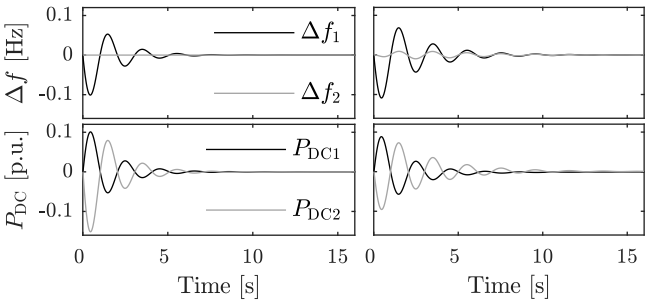

(a) Decoupling Control (b) $\mathcal{H}_2$ Optimal Control

Fig. 4. Comparing decoupling and $\mathcal{H}_2$ optimal control in a uneven system configuration.

Remark 3: The $\mathcal{H}_2$ synthesis yields a controller similar to that of the decentralized controller (4) (with a band pass-filter) as seen in Fig. 2d. This is because the decoupling controller in the one-sided configuration decouples the system by controlling one dc link in the wrong direction. Since this decoupling control action counteracts disturbance attenuation this will not be the $\mathcal{H}_2$ optimal control method.

When the HVDC terminals are rearranged into a *uneven configuration* (see Section III-E) where,

- relative dc bus locations $a_{11} = a_{21} = 0.2$, $a_{12} = 0.7$, and $a_{22} = 0.3$,

we find that the $\mathcal{H}_2$ optimal controller resembles a decoupling controller as seen in Fig. 4. This is because disturbance attenuation and decoupling requires the same dc power direction. Similarly, if the system is ill-conditioned, the $\mathcal{H}_2$ optimal controller will resemble the single-line controller since cancellation of multivariable interactions will require too much input usage.

E. Consequences of DC Link Failure, $N-1$ Stability Criterion

With single-line control, a disconnection will lead to a weaker control action. In the case of decentralized control, disconnection of one HVDC link will leave one of the networks outside the feedback-loop altogether. Neither of the mentioned contingencies will destabilize the system so the $N-1$ criterion (w.r.t. the HVDC control) is fulfilled without additional safety actions. With the decoupling controller however, it can be shown (see Appendix) that if

$$-\text{sgn}(b_{22})b_{21}b_{12} > 0,\ \text{sgn}(b_{11}) \text{ and } \text{sgn}(k) \triangleq 1 \qquad (7)$$

[1]Choosing $W = G^{-1}$ would result in $\tilde{G} = I$. To make the controller proper however, additional poles would have to be added to K.

is violated, the system will always be destabilized by the HVDC controller following a dc link failure. If the inherent damping is weak, then instability is likely to ensue if no safety measures are taken. Since (7) requires that one link has opposite sign in b_{ih} relative to the others, placing it on the other side of the electrical midpoint, (e.g. Fig. 5.2) this will henceforth be referred to as an *uneven configuration*.

Measurement Failure: If the system experiencing measurement failure is open-loop stable then instability does not ensue.

Communication Failure: If a measurement signal fails to reach one of the dc link controllers and (7) is violated, then one link will provide negative feedback while the other link provides positive feedback. If the communication to the negative feedback link fails then the system will be destabilized.

IV. Two HVDC-Interconnected Nordic-32 Models

Two HVDC-interconnected Nordic-32 Cigré test systems (N32) [16] are implemented in Simulink. The N32 model is a system with large power transfers from the hydro dominated north and external areas (lumped into north area) to loads in the central and southwestern areas (lumped into the south area) where a large amount of thermal power is installed. The model shows a 0.5 Hz interarea mode between the north and south areas. For illustrative purposes, the damping of this mode is reduced to roughly 1% by modifying the PSS of the machines at buses 4072 and 1042. Since we want to investigate

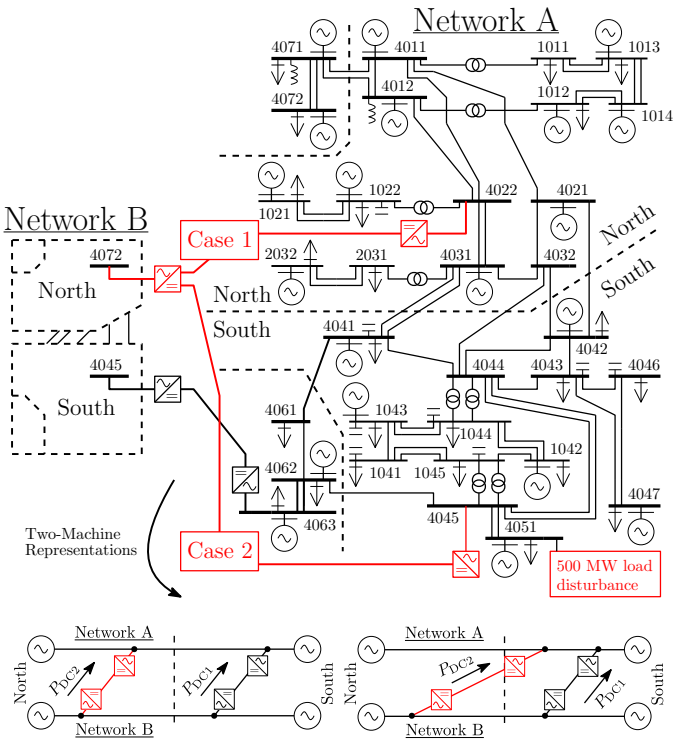

Fig. 5. Two HVDC-interconnected N32 networks. The frequency of the interarea mode in network A and B are 0.5 Hz and 0.6 Hz respectively.

stability issues following dc link failure, the system needs to be controllable from a single HVDC link. This is achieved by adjusting the interarea mode of network B to 0.6 Hz by scaling down system inertia.

The two N32 models are interconnected using two different HVDC-configurations, as seen in Fig. 5. A decoupling controller is tuned for each configuration using the procedure described in Section III-C and proportional feedback gain is set to 1,000 MW Hz^{-1}. Relative machine speed is estimated[2] from machine speed measurements as illustrated in Fig. 6.

The dynamical response following a 500 MW load disturbance (duration 1–2 s) at bus 4051 is simulated and the effect of dc link failure is investigated.

Case 1, Two-Sided HVDC-Configuration: The dc terminals are placed on both side of the electrical mid point in each system as shown in Fig.5.1. Similar to the one-sided configuration in Fig. 1 this violates the N-1 stability criterion (7). Thus, disconnection of one HVDC link lead to instability as shown in Fig. 7.

Case 2, Uneven HVDC-Configuration: The dc terminals are placed unevenly in the two systems as shown in Fig. 5.2 such that the $N-1$ stability criterion (7) is fulfilled. Therefore, disconnection of one HVDC link does not cause instability. Additionally, the system is controllable from one HVDC link. Thus the HVDC control still stabilizes the system as seen in Fig. 8.

[2]The state variables' participation [1] in the eigenvalues corresponding to the interarea modes is taken into account.

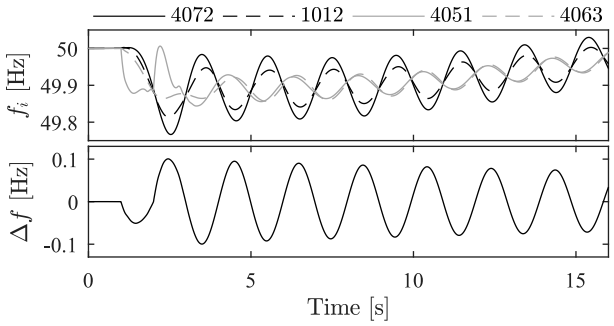

Fig. 6. Four machine speed measurements (top) following a 500 MW load disturbance without HVDC POD control. The relative machine speed (bottom) is estimated from measurements at all the machines.

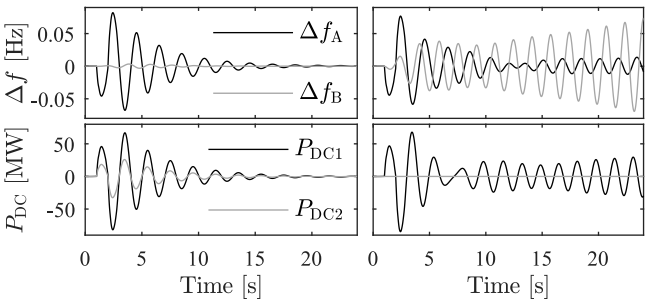

Fig. 7. Case 1: Two-sided HVDC-configuration, Fig. 5.1. Relative machine speeds and HVDC power injections following a 500 MW load disturbance.

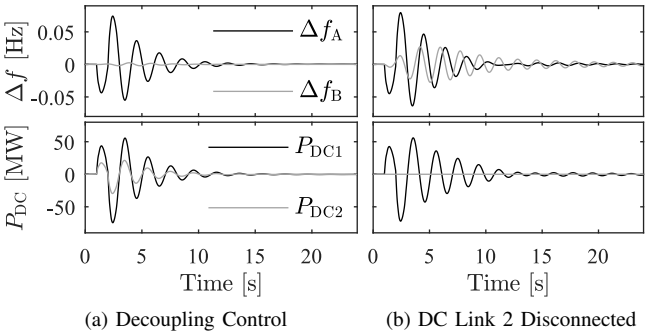

Fig. 8. Case 2: Uneven HVDC-configuration, Fig. 5.2. Relative machine speeds and HVDC power injections following a 500 MW load disturbance.

V. Conclusions

Coordinated control of two HVDC link interconnecting two asynchronous ac grids have been studied using a simplified two-machine model and a detailed model of two HVDC-interconnected N32 models. The analysis shows that if the $N-1$ stability criterion (7) holds, then a decoupling controller is a good choice. It is also shown that decoupling of oscillatory modes can be done using a proportional controller. If (7) is violated, then a decentralized control is preferred if the system is well conditioned. If not, then a single-line controller (uniform control of the HVDC links) is the appropriate choice since cancellation of multivariable interaction will require too much input usage. In all of these cases, the $\mathcal{H}_2$ optimal controller

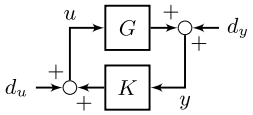

Fig. 9. Closed loop system used to study internal stability.

will give the preferable control structure.

In this study we considered POD of one dominant interarea mode in each ac network. In future work the study will be extended to incorporate more HVDC links and the interaction between multiple electro mechanical modes.

APPENDIX

A system is internally stable if all the four closed-loop transfer functions in Fig. 9,

$$\begin{aligned} u &= (I - KG)^{-1}d_u + K(I - GK)^{-1}d_y \\ y &= G(I - KG)^{-1}d_u + (I - GK)^{-1}d_y, \end{aligned} \tag{8}$$

from external input disturbances d_u and output disturbances d_y, are stable. Since G and K ((2) and (6) respectively) contains no RHP poles it is sufficient to show that one of the transfer functions in (8) are stable [17]. If we assume failure of HVDC link 2, then internal stability can be assessed by picking the (siso) internal sensitivity function from d_{u1} to u_1

$$S_{I1} = \frac{(s^2 + \Omega_1^2)(s^2 + \Omega_2^2)}{p(s)}.$$

Internal stability can then be assessed from the pole polynomial

$$\begin{aligned} p(s) = s^4 + s^3(b_1 + b_2) + s^2(\Omega_1^2 + \Omega_2^2) \\ + s(b_1\Omega_2^2 + b_2\Omega_1^2) + \Omega_1^2\Omega_2^2. \end{aligned} \tag{9}$$

where w_{11} and w_{12} are constant elements from the top row of the decoupling pre-compensator (5), and

$$b_1 \triangleq kb_{11}w_{11}, \quad b_2 \triangleq \text{sgn}(b_{22})kb_{21}w_{12}. \tag{10}$$

Routh's algorithm provide a necessary and sufficient condition for stability of the system [18]. For the pole polynomial (9) to have negative-real-part roots its required that

$$1 > 0$$

$$b_1 + b_2 > 0 \tag{11}$$

$$\frac{b_1\Omega_1^2 + b_2\Omega_2^2}{b_1 + b_2} > 0 \tag{12}$$

$$\frac{b_1b_2(\Omega_1^2 - \Omega_2^2)^2}{b_1\Omega_1^2 + b_2\Omega_2^2} > 0 \tag{13}$$

$$\Omega_1^2\Omega_2^2 > 0.$$

With (5) and (10) stability condition (11) becomes

$$b_1 + b_2 = kb_{11} - \text{sgn}(b_{22})kb_{21}\frac{b_{12}}{b_{11}} > 0 \tag{14}$$

thus the condition simplifies to $b_{11}^2 > \text{sgn}(b_{22})b_{21}b_{12}$. Similarly, condition (12) boils down to

$$b_{11}^2 > \text{sgn}(b_{22})\frac{\Omega_2^2}{\Omega_1^2}b_{21}b_{12}. \tag{15}$$

If (14), and thus (15) holds then the pole polynomial (9) have negative-real-part roots if (from (13))

$$b_1b_2 = k^2b_{11}\left(-\text{sgn}(b_{22})b_{21}\frac{b_{12}}{b_{11}}\right) > 0.$$

This gives the $N - 1$ stability criterion

$$-\text{sgn}(b_{22})b_{21}b_{12} > 0, \ \text{sgn}(b_{11}) \text{ and } \text{sgn}(k) \triangleq 1. \tag{7}$$

If $\Omega_1 = \Omega_2$, b_{12}, or b_{21} the system is not controllable and thus cannot be stabilized nor destabilized by the remaining HVDC link.

REFERENCES

[1] P. Kundur, *Power System Stability and Control*. New York: McGraw-Hill, 1994.

[2] M. A. Elizondo, R. Fan, H. Kirkham, M. Ghosal, F. Wilches-Bernal, D. A. Schoenwald, and J. Lian, "Interarea oscillation damping control using high voltage dc transmission: A survey," *IEEE Transactions on Power Systems*, May 2018.

[3] H. Latorre and M. Ghandhari, "Improvement of power system stability by using a VSC-HVdc," *International Journal of Electrical Power & Energy Systems*, vol. 33, no. 2, pp. 332–339, Feb. 2011.

[4] W. Winter, K. Elkington, G. Bareux, and J. Kostevc, "Pushing the limits: Europe's new grid: Innovative tools to combat transmission bottlenecks and reduced inertia," *IEEE Power and Energy Magazine*, vol. 13, no. 1, pp. 60–74, Jan. 2015.

[5] T. Smed and G. Andersson, "Utilizing HVDC to damp power oscillations," *IEEE Transactions on Power Delivery*, vol. 8, no. 2, pp. 620–627, Apr. 1993.

[6] R. L. Cresap, W. A. Mittelstadt, D. N. Scott, and C. W. Taylor, "Operating experience with modulation of the Pacific HVDC Intertie," *IEEE Transactions on Power Apparatus and Systems*, vol. PAS-97, no. 4, pp. 1053–1059, Jul. 1978.

[7] D. Trudnowski, D. Kosterev, and J. Undrill, "PDCI damping control analysis for the western North American power system," in *IEEE Power Energy Society General Meeting*, Vancouver, Canada, 2013.

[8] R. Preece, J. V. Milanovic, A. M. Almutairi, and O. Marjanovic, "Probabilistic evaluation of damping controller in networks with multiple VSC-HVDC lines," *IEEE Transactions on Power Systems*, vol. 28, no. 1, pp. 367–376, Feb. 2013.

[9] A. Fuchs and M. Morari, "Placement of HVDC links for power grid stabilization during transients," in *IEEE PowerTech*, Grenoble, France, 2013.

[10] R. Eriksson, "A new control structure for multiterminal dc grids to damp interarea oscillations," *IEEE Transactions on Power Delivery*, vol. 31, no. 3, pp. 990–998, Jun. 2016.

[11] Y. Li, Z. Xu, J. Østergaard, and D. J. Hill, "Coordinated control strategies for offshore wind farm integration via VSC-HVDC for system frequency support," *IEEE Transactions on Energy Conversion*, vol. 32, no. 3, pp. 843–856, Sep. 2017.

[12] W. Du, Q. Fu, and H. Wang, "Strong dynamic interactions between multi-terminal dc network and ac power systems caused by open-loop modal coupling," *IET Generation, Transmission & Distribution*, vol. 11, no. 9, pp. 2362–2374, Jun. 2017.

[13] L. Harnefors, N. Johansson, and L. Zhang, "Impact on interarea modes of fast HVDC primary frequency control," *IEEE Transactions on Power Systems*, vol. 32, no. 2, pp. 1350–1358, Mar. 2017.

[14] J. Björk, K. H. Johansson, and L. Harnefors, "Fundamental performance limitations in utilizing HVDC to damp interarea modes," submitted for publication.

[15] S. Skogestad and I. Postlethwaite, *Multivariable Feedback Control: Analysis and Design*, 2nd ed. Chichester, England: Wiley, 2005.

[16] M. Stubbe, "Long term dynamics phase II final report," Cigre, Tech. Rep. Task Force 38.08.08, Mar. 1995.

[17] K. Zhou, *Robust and Optimal Control*. Englewood Cliffs, NJ: Prentice Hall, 1996.

[18] T. Glad and L. Ljung, *Reglerteknik: Grundläggande teori*, 4th ed. Lund, Sweden: Studentlitteratur, 2006.